



# Perfusion contrast-enhanced ultrasound to predict early lymph-node metastasis in breast cancer

Naoko Mori<sup>1</sup> · Shunji Mugikura<sup>1</sup> · Minoru Miyashita<sup>2</sup> · Yumiko Kudo<sup>3</sup> · Mikiko Suzuki<sup>1</sup> · Li Li<sup>1</sup> · Yu Mori<sup>4</sup> · Shoki Takahashi<sup>1</sup> · Kei Takase<sup>1</sup>

Received: 10 July 2018 / Accepted: 12 November 2018 / Published online: 20 November 2018  
© Japan Radiological Society 2018

## Abstract

**Purpose** To evaluate whether quantitative analysis of perfusion contrast-enhanced ultrasound (CE-US) could predict early lymph-node (LN) metastasis in clinically node-negative breast cancer.

**Materials and methods** In this prospective study, 64 breast cancer patients were selected for perfusion CE-US imaging. Regions of interest were placed where the strongest and weakest signal increases were found to obtain peak intensities (PIs;  $PI_{max}$  and  $PI_{min}$ , respectively) for time–intensity curve analyzes. The PI difference and PI ratio were calculated as follows: PI difference =  $PI_{max} - PI_{min}$ ; PI ratio =  $PI_{max}/PI_{min}$ .

**Results** Forty-seven cases were histologically diagnosed as negative for LN metastasis and 17 were positive. There was a significant difference in  $PI_{min}$  and the PI ratio between the LN-negative and -positive metastasis groups ( $p = 0.0053$  and  $0.0082$ , respectively). Receiver-operating curve analysis revealed that the area under the curve of  $PI_{min}$  and the PI ratio were 0.73 and 0.72, respectively. The most effective threshold for the PI ratio was 1.52, and the sensitivity, specificity, positive predictive value, and negative predictive value were 59% (10/17), 87% (41/47), 63% (10/16), and 85% (41/48), respectively.

**Conclusions** Parameters from the quantitative analysis of perfusion CE-US imaging showed significant differences between the LN-negative and -positive metastasis groups in clinically node-negative breast cancer.

**Keywords** Breast cancer · Lymph-node metastasis · Ultrasound · Contrast-enhanced ultrasound · Microbubble

## Abbreviations

CE-US Contrast-enhanced ultrasound  
LN Lymph node  
PIs Peak intensities

SLNB Sentinel LN biopsy  
TIC Time–intensity curve  
MVD Microvessel density  
AUC Area under the curve

✉ Naoko Mori  
naokomori7127@gmail.com

Shunji Mugikura  
mugi844@gmail.com

Minoru Miyashita  
atihsayim8m8@med.tohoku.ac.jp

Yumiko Kudo  
yumiko4463@yahoo.co.jp

Mikiko Suzuki  
mikikomatsumura18@gmail.com

Li Li  
lilijanzhen05@gmail.com

Yu Mori  
irom100@gmail.com

Shoki Takahashi  
t-shoki@rad.med.tohoku.ac.jp

Kei Takase  
ktakase@rad.med.tohoku.ac.jp

<sup>1</sup> Department of Diagnostic Radiology, Tohoku University Graduate School of Medicine, Seiryō 1-1, Sendai 980-8574, Japan

<sup>2</sup> Department of Surgical Oncology, Tohoku University Graduate School of Medicine, Seiryō 1-1, Sendai 980-8574, Japan

<sup>3</sup> Department of Physiological Laboratory Center, Tohoku University Hospital, Seiryō 1-1, Sendai 980-8574, Japan

<sup>4</sup> Department of Orthopedic Surgery, Tohoku University Graduate School of Medicine, Seiryō 1-1, Sendai 980-8574, Japan

|     |                                    |
|-----|------------------------------------|
| ROI | Regions of interest                |
| ICC | Interclass correlation coefficient |
| ROC | Receiver-operating characteristic  |

## Introduction

Axillary lymph-node (LN) status is an important prognostic factor in newly diagnosed breast cancer patients, as strong correlations between LN metastasis and overall and disease-free survival have been reported [1–3]. If LN status was preoperatively diagnosed, sentinel LN biopsy (SLNB) could be avoided for node-negative patients [4], and neoadjuvant chemotherapy could be suggested for node-positive patients [5]. Furthermore, the American College of Surgeons Oncology Group Z0011 trial showed that survival rate with the use of SLND alone did not inferior to that with axillary LN dissection among patients with limited SLN metastases treated with breast conservation and systemic therapy [6].

Several attempts have been made to evaluate LN metastasis using the conventional imaging techniques such as ultrasonography (US), computed tomography (CT), and magnetic resonance imaging (MRI). Using B-mode US, cortical thickening, the absence of an echogenic hilum, a rounded shape, or a peripheral capsular vascularization in Doppler imaging are considered signs of metastatic LNs [7–10]. Using CT or MRI, irregular cortical thickening and size increase in thickness have been reported to correlate with the presence of LN metastasis [11, 12]. Large LN metastases with extranodal invasion can be detected by morphologic changes or size increase through US, CT, or MRI; however, early or small metastases without morphologic changes or size increases might be misdiagnosed using the conventional imaging. A novel imaging technique to detect clinically negative LN metastases is needed.

Microbubble perfusion contrast-enhanced ultrasound (CE-US) imaging was developed to evaluate tumor vasculature and perfusion. Microbubbles remain solely intravascular in nature, because they have a diameter of 2–3  $\mu\text{m}$  and cannot pass through the vascular endothelial interspace, thus enabling direct evaluation of the tumor vasculature and blood vessel volume [13, 14]. Li et al. reported that changes in blood vessel volume measured by perfusion CE-US were useful for diagnosing the early LN metastases in an animal model [15, 16]. In a human study, Rubaltelli et al. reported that LN metastases were characterized by hypo-perfused areas in perfusion CE-US imaging, and that the difference between maximum and minimum signal intensity values was greater in metastatic LNs than non-metastatic LNs [17, 18].

Several reports studying the methods of quantitatively analyzing perfusion CE-US data have shown that parameters taken from time–intensity curve (TIC) analyzes are correlated with histological microvessel density (MVD) [19–22].

The peak intensity (PI) and area under the curve (AUC) were significantly correlated with MVD in animal models [20]. In human study, the PI obtained from TIC analyzes of in vivo perfusion CE-US imaging data significantly correlated with MVD [21, 22].

We hypothesized that TIC analysis of perfusion CE-US imaging data could indicate the presence of hypo-perfused LN areas, which could be used to predict the early breast cancer LN metastasis. The purpose of this study was to evaluate whether quantitative analysis of perfusion CE-US data could predict the early LN metastasis in clinically node-negative breast cancer.

## Materials and methods

### Patients

Our Institutional Review Board approved this prospective study and written informed consent was obtained from all patients prior to enrollment. Between August 2014 and August 2017, 69 consecutive patients underwent preoperative perfusion CE-US followed by mastectomy or lumpectomy. The inclusion criteria were written informed consent, invasive breast cancer diagnosed by preoperative biopsy, and the absence of swollen LNs in the conventional CT, MRI, or US (clinically node-negative breast cancer). The swollen LNs were defined as LNs with morphologic changes such as cortical thickening, rounded shape, hypoechoic, and absence of fatty hilum [8, 23]. The exclusion criteria were ductal carcinoma in situ diagnosed by preoperative biopsy, for which the clinical significance of evaluating LNs is unknown [24], and prior neoadjuvant treatment, which could change LN biology. One patient whose CE-US data were not saved due to equipment error and four patients whose axillary LNs were not detected by B-mode imaging were excluded from the analysis. Thus, this prospective study examined 64 LNs from 64 female patients with unilateral breast carcinomas [median age 58 years (range 35–77); median body weight 50 kg (range 45–75)].

### US examination

US examinations were performed the day before surgery by a single radiologist with 7 years of experience in breast CE-US. Grayscale conventional US imaging was performed for the breast tumor and axillary LN with an Aplio 500 (Toshiba Medical Systems, Tochigi, Japan) with a 10 MHz linear transducer. For axillary evaluations, the LN with the largest cross-sectional area was selected to obtain the CE-US data using B-mode imaging. CE-US was performed for the LN with a single plane with the largest cross-sectional area using the same unit, with 5.5–7.5 MHz linear transducer in dual-screen mode

that simultaneously displayed both the conventional B-mode and CE-US mode images. The transducer was softly laid on the skin to not compress the tissue or collapse the vascular lumen. The machine parameters were adjusted, so that the mechanical index was 0.18–0.2, the frame rate was 17 frames per second (fps), and the gain was 80–100 dB. No parameters were changed during examinations.

The contrast agent used in this study was Sonazoid (Dai-ichi Sankyo, Tokyo, Japan), a lipid-stabilized suspension of perflubutane microbubbles. The contents of each vial (16  $\mu$ l of perflubutane microbubbles) were resuspended in 2 ml of water for injection. Each patient received a single injection of 0.015 ml/kg of the reconstituted suspension into a forearm vein followed by a 10 ml saline flush at a slow injection speed, and then, continuous 75-s imaging from injection was obtained as a video of DICOM data. Patients were told to keep as still as possible during the examination.

### Evaluating breast tumors and LNs

Breast tumors and LNs were initially evaluated using the conventional US imaging by the consensus of two radiologists (7 and 2 years of experience in breast US) according to the American College of Radiology Breast Imaging Reporting and Data System US criteria (American College of Radiology, 2013) [25]. The criteria included the size of the breast tumor, diameter of major axis, cortical thickness, shape, patterns of cortical thickening, margins, and hilar compression of LNs.

### Quantitative analysis of LN perfusion CE-US

Postprocessed DICOM data from US imaging were analyzed with Image J [1.51q 18, National Institutes of Health (NIH)]. Quantitative TIC parameters were obtained with previously published online NIH Image J tools [22, 26].

The same two radiologists visually identified the 64 LNs. To obtain quantitative parameters, three regions of interest (ROIs) were placed where the strongest enhancement was found inside the LNs at the peak phase of the CE-US, which was observed 20–40 s after injecting contrast agent (Fig. 1a). A TIC was generated from the ROIs (Fig. 1b), and the PI of each ROI was calculated from the curve. The maximum PI value of the three ROIs was then recorded as  $PI_{max}$ . For  $PI_{min}$ , three ROIs were placed where the weakest enhancement was found at the peak phase (Fig. 1a) to generate TIC. PI of each ROI was calculated from the curve and the minimum PI value of the three ROIs was recorded as  $PI_{min}$ . Then, we obtained the following derivation for a diagnostic parameter that represented the heterogeneity of LN enhancement:

$$PI \text{ difference} = PI_{max} - PI_{min} \quad (1)$$

$$PI \text{ ratio} = PI_{max}/PI_{min} \quad (2)$$

$PI_{max}$ ,  $PI_{min}$ , the PI difference, and PI ratio for each reader were then analyzed using interclass correlation coefficient (ICC). Finally,  $PI_{max}$ ,  $PI_{min}$ , the PI difference, and PI ratio were compared between the LN-negative and -positive metastasis groups.

### Visual analysis of LN CE-US

The same two radiologists, blinded to clinical information, also independently visually evaluated the presence of perfusion defects (negative or positive) within LNs on perfusion CE-US: negative was scored when the contrast-enhancement in LNs was homogeneous with high signal enhancement (Fig. 2a); positive was scored when the contrast-enhancement in LNs was heterogeneous with obvious perfusion defects (Fig. 2b). Visual evaluations of perfusion defects by each reader were analyzed using kappa statistics. The visual evaluation results were compared between the LN-negative and -positive metastatic groups.

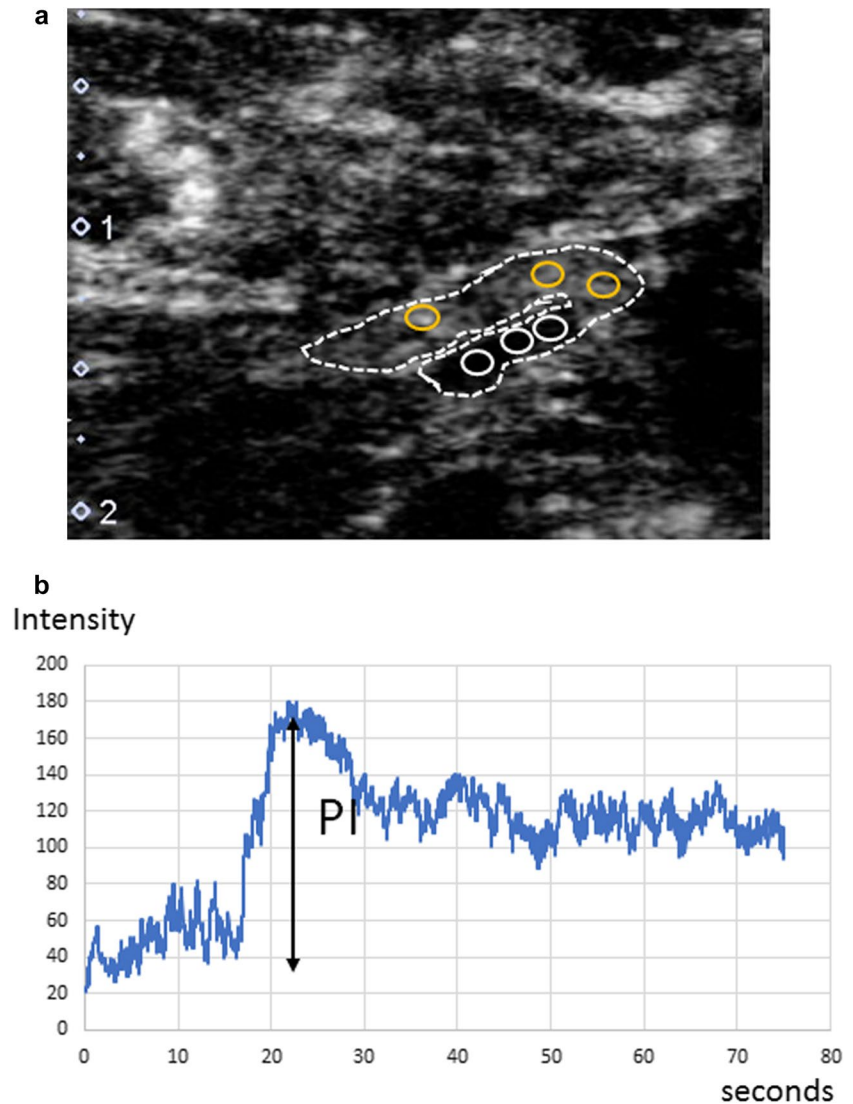
### Pathological evaluation

All patients underwent sentinel LN biopsy followed by mastectomies or lumpectomies; surgical specimens were then prepared for histological evaluation. Specimens were fixed in 10% formaldehyde, and 2- $\mu$ m sections were taken every 1.5 mm. An experienced pathologist evaluated the LN specimens based on the World Health Organization histological classifications of breast tumors. Metastatic nests > 0.2 mm in diameter were scored as LN-positive metastases.

### Statistical analysis

Mann–Whitney *U* tests were used to compare age, breast tumor diameter, diameter of major axis, and cortical thickness of LNs, nuclear grade, Ki-67 labeling index,  $PI_{max}$ ,  $PI_{min}$ , PI difference, and PI ratio between the LN-negative and -positive metastasis groups. Chi-square tests were used to compare shapes, cortical thickening patterns, and histological types. Fisher's exact test was used to compare clinical stage, margins, hilar compression, immunohistochemical findings of tumor including the status of estrogen receptor, progesterone receptor and human epidermal growth factor receptor 2 (HER2), and visual analyzes of perfusion defects (negative or positive). The inter-observer reliability of  $PI_{max}$ ,  $PI_{min}$ , PI difference, and PI ratio results was assessed using ICCs. The inter-observer reliability of visual evaluation results (positive or negative for the presence of perfusion defects) was assessed using kappa statistics. An *r* of 1.0 indicated perfect agreement; 0.81–0.99, almost perfect agreement; 0.61–0.80, substantial agreement; 0.41–0.60, moderate agreement; 0.21–0.40, fair agreement;  $\leq$  0.20, slight agreement [27]. The performance of  $PI_{min}$  and PI ratio

**Fig. 1** Methods for placing regions of interest (ROIs) in lymph nodes (LNs) and acquiring time–intensity curves (TICs) for contrast-enhanced ultrasound (CE-US) imaging in a 60-year-old woman preoperatively diagnosed with invasive breast carcinoma. The status of LN was diagnosed as positive with 4 mm metastatic nest by surgery. **a** The harmonic CE-US imaging at the peak phase. Inside the LN (dotted line), three ROIs (orange) were placed where the strongest enhancement was found. The other three ROIs (white) were placed where the weakest enhancement was found. **b** TICs were generated from the ROIs with time on the *x*-axis and signal intensity on the *y*-axis. Peak intensity (PI) was measured from the TIC. The maximum PI value from the three ROIs with the strongest enhancement was recorded as  $PI_{max}$ . The minimum PI value from the three ROIs with the weakest enhancement was recorded as  $PI_{min}$  (colour figure online)



in differentiating the LN-negative and -positive metastasis groups was evaluated using receiver-operating characteristic (ROC) analysis and AUC. Statistical analyzes were performed using commercial software (JMP Pro 13, SAS Institute, Cary, NC, USA).  $p < 0.05$  was considered significant. After Bonferroni correction of 5 multiple comparisons, the critical value became  $< 0.01$  ( $0.05/5$ ).

## Results

Fourteen breast lesions were treated by mastectomy and the other 50 lesions were treated by lumpectomy. SLNB was performed for all patients: histological diagnoses were negative for 47 cases (the LN-negative metastasis group) and positive for 17 cases (the LN-positive metastasis group). In LN-negative metastasis group, a median of one sentinel LNs (range 1–5) per patient was sampled at SLNB and no LN

was diagnosed with metastasis. In LN-positive metastasis group, a median of one sentinel LNs (range 1–5) per patient was sampled at SLNB and a median of one LN (range 1–3) was diagnosed with metastasis. Axillary LN dissections were performed for all patients in the LN-positive metastasis group. There were no positive LN metastases by histology in the four patients whose axillary LNs were undetectable by B-mode imaging; these patients were still excluded from the analysis.

Patient characteristics, conventional US imaging findings according to the Breast Imaging Reporting and Data System (American College of Radiology, 2013) [25], and histopathological results obtained from surgical specimen are shown in Table 1. No statistically significant differences were found between the LN-negative and -positive metastasis groups with respect to age, clinical stage, US findings (breast tumor diameter, diameter of major axis, cortical thickness, shape, cortical thickening patterns,

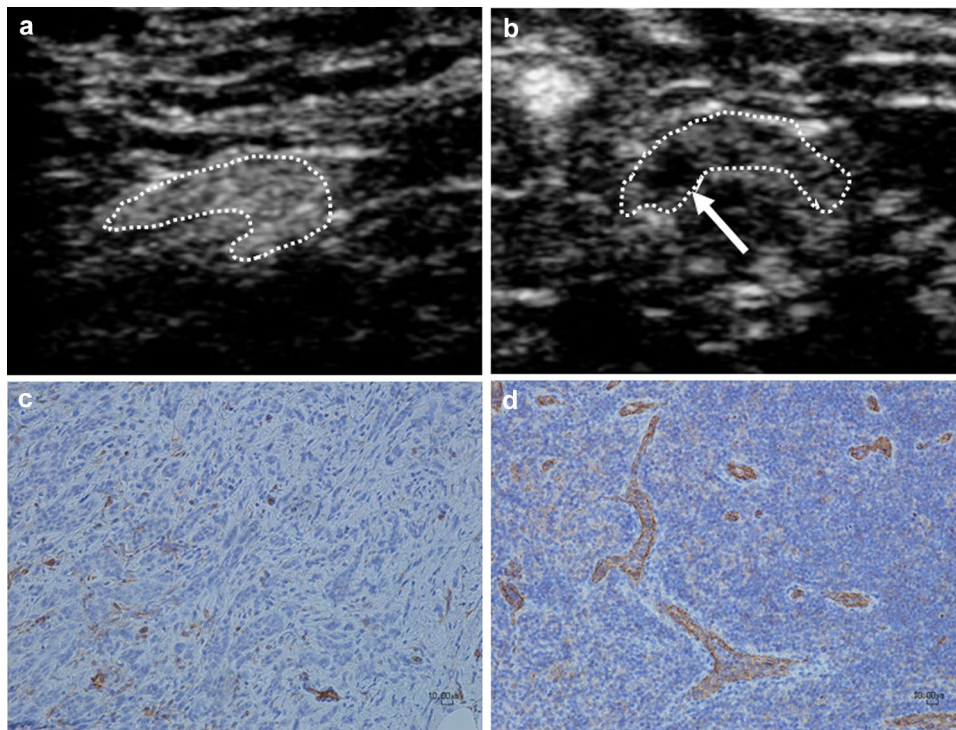


**Fig. 2** Visual assessment of the presence of perfusion defects (negative or positive). **a** A 36-year-old woman preoperatively diagnosed with invasive breast carcinoma. The status of LN was diagnosed as negative metastasis by surgery. Perfusion contrast-enhanced ultrasound (CE-US) imaging of a lymph node (LN) (dotted line) showing homogeneous enhancement, which was interpreted as negative for perfusion defects. **b–d** A 47-year-old woman preoperatively diagnosed with invasive breast carcinoma. The status of LN was diag-

nosed as positive with 7 mm metastatic nest by surgery. Perfusion CE-US of an LN (dotted line) showing heterogeneous enhancement with an obvious perfusion defect (arrow), which was interpreted as positive for perfusion defects (**b**). Mouse anti-human CD31 monoclonal antibody (Dako Cytomation, Glostrup, Denmark) was used to evaluate the vascularity of LN immunohistochemically (**c**, **d**). The area with metastatic deposits (**c**) was less vascularized than that with normal LN parenchyma (**d**) ( $\times 200$  field)

margin, and hilar compression of LNs), and histology of breast tumor (histological type, nuclear grade, immunohistological findings of tumor, and Ki67 labeling index).

For the agreement between the readers with respect to their quantitative analysis of CE-US, ICCs of  $PI_{max}$ , PI difference, and PI ratio were 0.72, 0.56, and 0.63, respectively, indicating substantial agreement. The ICCs of  $PI_{min}$  was 0.83, indicating almost perfect agreement.

There was a significant difference in  $PI_{min}$  and the PI ratio between the LN-negative and -positive metastasis groups ( $p = 0.0053$  and  $0.0082$ , respectively, Table 2), while no significant difference was found in  $PI_{max}$  or the PI difference ( $p = 0.29$  and  $0.019$ , respectively, Table 2). ROC curve analysis revealed that the AUC of  $PI_{min}$  and the PI ratio were 0.73 and 0.72, respectively (Fig. 3a, b). The most effective threshold for  $PI_{min}$  was the 112 signal intensity, and the sensitivity, specificity, positive predictive value, and negative predictive value were 94% (15/17), 45% (21/47), 38% (16/42), and 71% (21/22), respectively. The most effective threshold for the PI ratio was 1.52, and the sensitivity, specificity, positive predictive value, and

negative predictive value were 59% (10/17), 87% (41/47), 63% (10/16), and 85% (41/48), respectively.

In evaluating the agreement between readers,  $\kappa$  for the visual evaluation of the presence of perfusion defects was 0.25, indicating fair agreement. Furthermore, no statistical significance was found in the visual analysis of perfusion defects (negative or positive) between the LN-negative and -positive metastasis groups ( $p = 0.11$ , Table 3).

## Discussion

In our results,  $PI_{min}$  showed almost perfect inter-observer reliability and PI ratio showed substantial agreement, and both showed significant differences between the LN-negative and -positive metastasis groups, while  $PI_{max}$ , the PI difference, and visual assessments of perfusion defects did not.

The PI ratio was obtained by dividing  $PI_{max}$  by  $PI_{min}$ , while  $PI_{min}$  is the original signal intensity. Original signal intensity measured from perfusion CE-US imaging including  $PI_{min}$  could be affected by differences between patients

**Table 1** Comparing patient and lesion [breast tumors and lymph node (LN)] characteristics between LN-negative and -positive metastasis groups

| Variables   | LN-negative metastasis group ( <i>n</i> = 47) | LN-positive metastasis group ( <i>n</i> = 17) | <i>p</i> |
|---|---|---|----------|
| Age (years): median (range)                           | 59 (36–76)                                    | 49 (35–77)                                    | 0.21     |
| Clinical stage ( <i>n</i> /%)                         |   |   | 0.08     |
| T1  | 40 (85)                                       | 11 (65)                                       |          |
| T2  | 7 (15)  | 6 (35)  |          |
| Ultrasound findings breast tumor                      |   |   |          |
| Diameter: median (range)                              | 14.5 (5.1–34.1)                               | 17.9 (5.5–30.8)                               | 0.07     |
| LN  |   |   |          |
| Diameter of major axis                                | 11.4 ± 5.2                                    | 10.8 ± 4.1                                    | 0.91     |
| Cortical thickness (mm)                               | 2.0 ± 0.7                                     | 2.5 ± 1.0                                     | 0.08     |
| Shape ( <i>n</i> (%))                                 |   |   | 0.31     |
| Oval  | 10 (21)                                       | 6 (35)  |          |
| Round   | 3 (6)   | 2 (12)  |          |
| Irregular   | 34 (72)                                       | 9 (53)  |          |
| Cortical thickening patterns                          |   |   | 0.43     |
| None  | 37 (79)                                       | 12 (71)                                       |          |
| Uniform   | 2 (4)   | 0 (0)   |          |
| Focal   | 8 (17)  | 5 (29)  |          |
| Margin  |   |   | 1        |
| Circumscribed   | 47 (100)                                      | 17 (100)                                      |          |
| Uncircumscribed                                       | 0 (0)   | 0 (0)   |          |
| Hilar compression                                     |   |   | 1        |
| Positive  | 1 (2)   | 0 (0)   |          |
| Negative  | 46 (98)                                       | 17 (100)                                      |          |
| Histology of breast tumor                             |   |   | 0.31     |
| Invasive ductal carcinoma not otherwise specified     | 44  | 14  |          |
| Invasive lobular carcinoma                            | 1   | 2   |          |
| Mucinous carcinoma                                    | 2   | 1   |          |
| Nuclear grade ( <i>n</i> (%))                         |   |   | 0.68     |
| Low   | 33 (70)                                       | 12 (71)                                       |          |
| Intermediate  | 3 (7)   | 4 (24)  |          |
| High  | 11 (23)                                       | 1 (5)   |          |
| Immunohistochemical findings of tumor ( <i>n</i> (%)) |   |   |          |
| Estrogen receptor                                     | Positive 41 (87) negative 6 (13)              | Positive 17 (100) negative 0 (0)              | 0.18     |
| Progesterone receptor                                 | Positive 38 (81) negative 9 (19)              | Positive 16 (94) negative 1 (6)               | 0.26     |
| HER2  | Positive 3 (6) negative 44 (94)               | Positive 0 (0) negative 17 (100)              | 0.55     |
| Ki-67 labeling index median (range)                   | 12 (0.02–77.5)                                | 15 (1–70)                                     | 0.47     |

*HER2* human epidermal growth factor receptor 2

**Table 2** Comparing quantitative parameters from contrast-enhanced ultrasound between the lymph-node (LN)-negative and -positive metastasis groups and the interclass correlation coefficient (ICC) of each parameter

|                        | LN-negative metastasis group ( <i>n</i> = 47) | LN-positive metastasis group ( <i>n</i> = 17) | <i>p</i> | AUC  | ICC               |
|------------------------|---|---|----------|------|-------------------|
| PI <sub>max</sub> (SI) | 129 ± 39                                      | 114 ± 30                                      | 0.29     | N/A  | 0.72 (0.52, 0.84) |
| PI <sub>min</sub> (SI) | 110 ± 42                                      | 73 ± 38                                       | 0.0053   | 0.73 | 0.83 (0.69, 0.90) |
| PI difference (SI)     | 18 ± 16                                       | 41 ± 37                                       | 0.019    | N/A  | 0.56 (0.23, 0.74) |
| PI ratio               | 1.2 ± 0.2                                     | 2.8 ± 4.2                                     | 0.0082   | 0.72 | 0.63 (0.36, 0.79) |

*PI* peak intensity

*SI* signal intensity

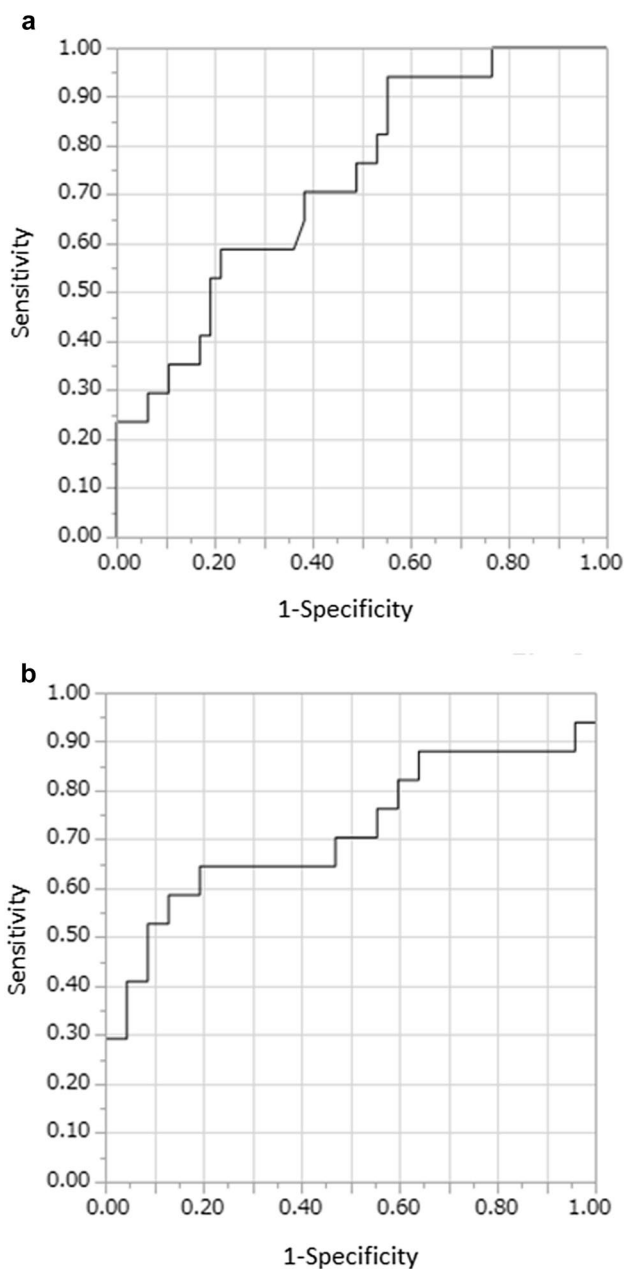


**Fig. 3** Graph of the receiver-operating curve (ROC) for  $tPI_{min}$  (a) and PI ratio (b) for differentiating LN-negative metastasis group and LN-positive metastasis group shows that the area under the ROC curve is 0.73 and 0.72, respectively

**Table 3** Comparing visual analyzes of perfusion defects (negative or positive) between the lymph-node (LN)-negative and positive groups

| Visual assessment of Perfusion defects | LN-negative metastasis group (n = 47) | LN-positive metastasis group (n = 17) |
|--|---------------------------------------|---------------------------------------|
| Negative                               | 36                                    | 9                                     |
| Positive                               | 11                                    | 8                                     |

and CE-US conditions, including the various depths of target lesions and gain adjustments, which is almost impossible to maintain with identical setting between different patients [28]. Therefore, we conclude that the PI ratio would be a more robust parameter than  $PI_{min}$  for differentiating LN-negative from LN-positive breast cancer.

In our study, no significant difference was found in PI difference, although there was a significant difference in PI ratio between LN-positive and LN-negative metastasis groups. PI ratio might be more sensitive to detect the difference in number than PI difference, which might have led to the difference in diagnostic utility.

According to the electron microscopic study by Gadre et al., normal and reactive LNs have intense vascularization with rich cortical capillary circulation [29]. In microangiographic examinations of animal models, Herman et al. revealed that metastatic deposits within the early stage metastatic LNs were hypo-vascularized [30]. In perfusion CE-US studies of human LNs [17, 18], Rubaltelli et al. showed that the hypo-perfused areas within metastatic LNs might be due to necrosis or the presence of metastatic tissue that was less vascularized than the normal LN parenchyma. Their study included swollen LNs in patients with neck squamous cell carcinomas, cutaneous melanomas, and breast carcinomas. Later, Ohta et al. reported that perfusion defects were observed in axillary LN metastases in breast cancer patients using perfusion CE-US [31]. While these studies examined swollen LNs, our study cohort was clinically node-negative breast cancer patients. Yet, we still found a significant difference between the LN-negative and -positive metastasis groups using quantitative parameters of perfusion CE-US imaging data:  $PI_{min}$  was significantly lower and the PI ratio was significantly higher in LN-positive group compared with the LN-negative group, while  $PI_{max}$  and the PI difference were not. These results indicate that metastatic deposits were also relatively hypo-vascularized in our study. We presume that hypo-perfused areas within clinically negative, but small metastatic LNs in our LN-positive group should have been histologically ascribed as relative hypo-vascularized metastatic deposits (Fig. 2c) compared with the normal LN parenchyma (Fig. 2d) rather than necrosis.

To our knowledge, there were no studies showing a significant difference in perfusion characteristics between metastatic LN and non-metastatic LN using CT or MRI in patients with breast cancer. The administered CT or MR contrast agent would not entirely remain within intravascular spaces, but a significant part of it would distribute into the surrounding extracellular spaces, while contrast agent of US (microbubble) remains solely intravascular in nature, because they have a diameter of 2–3  $\mu m$  and would not pass through the vascular endothelial interspace, thus enabling direct evaluation of the vasculature [13, 14]. We speculate that perfusion CE-US might be more appropriate to detect

the hypo-vascularized metastatic deposit than CT or MRI. Regarding the method to use contrast agent of CE-US in breast cancer patients, a method to localize sentinel LNs by visualizing lymphatic channels was proposed in animal model by Goldberg et al. [32], and later, the same method with sub-areolar injection of contrast agent in human (lymphangiographic CE-US) has been proposed [33, 34]. Zhao et al. used this method and reported that the enhancement pattern of sentinel LNs facilitated the identification of metastases [35]. However, the diagnostic performance for sentinel LN metastases may not be satisfactory (sensitivity, specificity, positive predictive value, and negative predictive value were 100%, 52.0%, 43.4%, and 100%, respectively). Our method of CE-US was performed by intravenous injection (perfusion CE-US). Its sensitivity, specificity, positive predictive value, and negative predictive value were 59%, 87%, 63%, and 85%, respectively. Comparing both CE-US methods, perfusion CE-US in this study had superiority in specificity and positive predictive value, whereas lymphangiographic CE-US in the Zhao et al.'s study had superiority in sensitivity and negative predictive value. One advantage of our CE-US method is that it is also applicable to the primary tumor, enabling the simultaneous evaluation of both primary tumors and LNs by CE-US. However, further studies conducting both methods on the same patients are needed to compare the clinical utility of both methods.

Axillary LN status is an important prognostic factor for newly diagnosed breast cancer patients. Therefore, sentinel LN biopsy has been recommended during surgery, because the diagnostic capability of the conventional imaging for LN metastases is not satisfactory [7, 36]. Our method of perfusion CE-US might enable the preoperative detection of the early LN metastasis, even in clinically node-negative patients. If the early LN metastasis was preoperatively suspected by perfusion CE-US, percutaneous LN biopsy could be performed to confirm the presence of LN metastasis. Then, for LN-positive cases, neoadjuvant chemotherapy or axillary dissection could be suggested, while the PI ratio showed a relatively high negative predictive value (85%) in our study. If the negative predictive value would be improved with technical development such as three-dimensional LN CE-US evaluations, perfusion CE-US might avoid sentinel LN biopsies in the future.

This study had several limitations. First, the sample size was small. Second, selecting the plane with the largest LN cross-sectional area was subjective, because we used a linear transducer with two-dimensional images. Selecting a single plane might miss small metastases, which would decrease the diagnostic strength. The false-negative results, that is cases with PI ratio under the threshold or no perfusion defect in visual analysis, even though there was LN metastasis by histology, might be due to the manner with selecting a single plane. Three-dimensional LN CE-US evaluations

would be preferable in the future. Third,  $PI_{min}$  and the PI ratio showed almost perfect and substantial inter-observer reliability, respectively. The inter-observer reliability of these quantitative parameters was higher than that of visual analyzes of perfusion defects, but was still unsatisfactory. To detect clinically negative metastatic LNs, more reproducible CE-US imaging techniques are needed. Fourth, we excluded patients with prior neoadjuvant treatment. Evaluation of LN metastasis after neoadjuvant treatment might clinically important. Further study including patients with neoadjuvant treatment would be necessary in the future. Finally, we could not perform point-to-point radiological–pathological analyzes for sentinel LNs; rather, we only did a patient-to-patient analysis. This was because we targeted LNs with the largest cross-sectional area on B-mode imaging, for which point-to-point correspondence was not obtained with sentinel LNs detected during surgery. Furthermore, there were cases who were evaluated as positive by perfusion CE-US, even though there was no LN metastasis by histology [false-positive results: quantitative analysis (13% (6/47))] and visual analysis [23% (11/47)], respectively. We speculated that mechanical artifacts or old inflammation in LN could cause these false-positive results. Further studies using intraoperative perfusion CE-US to correlate the findings with histology might be needed.

In conclusion, the parameters from the quantitative analyzes of LN CE-US imaging showed significant differences between the LN-negative and -positive metastasis groups in clinically node-negative breast cancer. We believe that our CE-US method will enable clinicians to detect small metastases in non-swollen LNs in breast cancer patients.

**Acknowledgements** This study was supported by JSPS KAKENHI 26461783 and 15K09913. The authors would like to thank Yumi Fujimoto in Tohoku University Hospital and Shomo Chou in Tohoku University for their kind support. We thank James P. Mahaffey, Ph.D., from Edanz Group ([www.edanzediting.com/ac](http://www.edanzediting.com/ac)) for editing a draft of this manuscript.

## Compliance with ethical standards

**Conflict of interest** Naoko Mori has nothing to disclose. Shunji Mugikura has nothing to disclose. Minoru Miyashita has nothing to disclose. Yumiko Kudo has nothing to disclose. Mikiko Suzuki has nothing to disclose. Li Li has nothing to disclose. Yu Mori has nothing to disclose. Shoki Takahashi has nothing to disclose. Kei Takase has nothing to disclose.

## References

1. Nemoto T, Vana J, Bedwani RN, Baker HW, McGregor FH, Murphy GP. Management and survival of female breast cancer: results of a national survey by the American College of Surgeons. *Cancer*. 1980;45(12):2917–24.



2. Banerjee M, George J, Song EY, et al. Tree-based model for breast cancer prognostication. *J Clin Oncol*. 2004;22:2567–75.
3. Cianfrocca M, Goldstein LJ. Prognostic and predictive factors in early-stage breast cancer. *Oncologist*. 2004;9:606–1.
4. Swenson KK. Comparison of side effects between sentinel lymph node and axillary lymph node dissection for breast cancer. *Ann Surg Oncol*. 2002;9:745–53.
5. Goldhirsch A, Winer EP, Coates AS, et al. Personalizing the treatment of women with early breast cancer: highlights of the St Gallen International Expert Consensus on the Primary Therapy of Early Breast Cancer 2013. *Ann Oncol*. 2013;24:2206–23.
6. Giuliano AE. Axillary dissection vs no axillary dissection in women with invasive breast cancer and sentinel node metastasis: a randomized clinical trial. *JAMA*. 2011;305:569.
7. Esen G, Gurses B, Yilmaz MH, et al. Gray scale and power Doppler US in the preoperative evaluation of axillary metastases in breast cancer patients with no palpable lymph nodes. *Eur Radiol*. 2005;15:1215–23.
8. Abe H, Schmidt RA, Kulkarni K, et al. Axillary lymph nodes suspicious for breast cancer metastasis: sampling with us-guided 14-gauge core-needle biopsy—clinical experience in 100 patients 1. *Radiology*. 2009;250:41–9.
9. Bedi DG, Krishnamurthy R, Krishnamurthy S, et al. Cortical morphologic features of axillary lymph nodes as a predictor of metastasis in breast cancer. *in vitro sonographic study*. *Am J Roentgenol*. 2008;191:646–52.
10. Abe H, Schmidt RA, Sennett CA, et al. US-guided core needle biopsy of axillary lymph nodes in patients with breast cancer: why and how to do it. *Radiographics*. 2007;27:S91–S99.
11. Scaranelo AM, Eiada R, Jacks LM, et al. Accuracy of unenhanced MR imaging in the detection of axillary lymph node metastasis: study of reproducibility and reliability. *Radiology*. 2012;262:425–34.
12. Shien T, Akashi-Tanaka S, Yoshida M, et al. Evaluation of axillary status in patients with breast cancer using thin-section CT. *Int J Clin Oncol*. 2008;13:314–9.
13. Loveless ME, Li X, Huamani J, et al. A method for assessing the microvasculature in a murine tumor model using contrast-enhanced ultrasonography. *J Ultrasound Med*. 2008;27:1699–709.
14. Szabó BK, Saracco A, Tánzos E, et al. Correlation of contrast-enhanced ultrasound kinetics with prognostic factors in invasive breast cancer. *Eur Radiol*. 2013;23:3228–36.
15. Li L, Mori S, Sakamoto M, et al. Mouse model of lymph node metastasis via afferent lymphatic vessels for development of imaging modalities. *PLoS One*. 2013;8:e55797.
16. Li L, Mori S, Kodama M, et al. Enhanced sonographic imaging to diagnose lymph node metastasis: importance of blood vessel volume and density. *Cancer Res*. 2013;73:2082–9.
17. Rubaltelli L, Beltrame V, Tregnaghi A, et al. Contrast-enhanced ultrasound for characterizing lymph nodes with focal cortical thickening in patients with cutaneous melanoma. *Am J Roentgenol*. 2011;196:W8–W12.
18. Rubaltelli L, Corradin S, Dorigo A, et al. Automated quantitative evaluation of lymph node perfusion on contrast-enhanced sonography. *Am J Roentgenol*. 2007;188:977–83.
19. Wan CF, Du J, Fang H, et al. Enhancement patterns and parameters of breast cancers at contrast-enhanced US: correlation with prognostic factors. *Radiology*. 2012;262:450–9.
20. Pitre-Champagnat S, Leguerney I, Bosq J, et al. Dynamic contrast-enhanced ultrasound parametric maps to evaluate intratumoral vascularization. *Investig Radiol*. 2015;50:212–7.
21. Du J, Li F-H, Fang H, et al. Correlation of real-time gray scale contrast-enhanced ultrasonography with microvessel density and vascular endothelial growth factor expression for assessment of angiogenesis in breast lesions. *J Ultrasound Med*. 2008;27:821–3.
22. Mori N, Mugikura S, Takahashi S, et al. Quantitative analysis of contrast-enhanced ultrasound imaging in invasive breast cancer: a novel technique to obtain histopathologic information of microvessel density. *Ultrasound Med Biol*. 2017;43:607–14.
23. Ecanow JS, Abe H, Newstead GM, et al. Axillary staging of breast cancer: what the radiologist should know. *Radiographics*. 2013;33:1589–612.
24. Murphy CD, Jones JL, Javid SH, et al. Do sentinel node micro-metastases predict recurrence risk in ductal carcinoma in situ and ductal carcinoma in situ with microinvasion? *Am J Surg*. 2008;196:566–8.
25. American College of Radiology. Breast imaging reporting and data system (BI-RADS). 5th ed. Reston: Reston American College of Radiology; 2013.
26. Schneider CA, Rasband WS, Eliceiri KW, et al. NIH Image to ImageJ: 25 years of image analysis. *Nat Methods*. 2012;9:671–5.
27. Landis JR, Koch GG. The measurement of observer agreement for categorical data. *Biometrics*. 1977;33:159.
28. Ignee A, Jedrejczyk M, Schuessler G, et al. Quantitative contrast enhanced ultrasound of the liver for time intensity curves—reliability and potential sources of errors. *Eur J Radiol*. 2010;73:153–8.
29. Gadre A, Briner W, O’Leary M. A scanning electron microscope study of the human cervical lymph node. *Acta Otolaryngol (Stockh.)*. 1994;114:87–90.
30. Herman PG, Kim C-S, de Sousa MA, et al. Microcirculation of the lymph node with metastases. *Am J Pathol*. 1976;85:333.
31. Ohta T, Nishioka M, Nakata N, et al. Five cases of axillary lymph node metastatic breast cancer on contrast-enhanced sonography. *J Ultrasound Med*. 2015;34:1131–7.
32. Goldberg BB, Merton DA, Liu J-B, et al. Contrast-enhanced sonographic imaging of lymphatic channels and sentinel lymph nodes. *J Ultrasound Med*. 2005;24:953–65.
33. Omoto K, Matsunaga H, Take N, et al. Sentinel node detection method using contrast-enhanced ultrasonography with sonazoid in breast cancer: preliminary clinical study. *Ultrasound Med Biol*. 2009;35:1249–56.
34. Cox K, Taylor-Phillips S, Sharma N, et al. Enhanced pre-operative axillary staging using intradermal microbubbles and contrast-enhanced ultrasound to detect and biopsy sentinel lymph nodes in breast cancer: a potential replacement for axillary surgery. *Br J Radiol*. 2018;91(1082):20170626.
35. Zhao J, Zhang J, Zhu Q-L, et al. The value of contrast-enhanced ultrasound for sentinel lymph node identification and characterisation in pre-operative breast cancer patients: a prospective study. *Eur Radiol*. 2018;28(4):1654–61.
36. Veronesi U, De Cicco C, Galimberti V, et al. A comparative study on the value of FDG-PET and sentinel node biopsy to identify occult axillary metastases. *Ann Oncol*. 2006;18:473–8.